Using Redundant Effectors to Trim a Compound Helicopter with Damaged Main Rotor Controls

Jean-Paul Reddinger
Ph.D. Candidate
Rensselaer Polytechnic Institute
Troy, NY

Farhan Gandhi
Professor
Rensselaer Polytechnic Institute
Troy, NY

ABSTRACT

Control of a helicopter's main rotor is typically accomplished through use of three hydraulic actuators that act on the non-rotating swashplate and position it to achieve any combination of collective and cyclic blade pitch. Failure of one of these servos can happen through loss of hydraulic pressure or by impingement of the piston within the hydraulic cylinder. For a compound helicopter with an articulated main rotor, a range of failed servo states (by piston impingement) are simulated in RCAS at hover, 100 kts, and 200 kts, to show the extent to which the compound effectors can generate additional forces and moments to maintain trimmed flight. After the loss of control of any of the three main rotor actuators in hover, the compound helicopter is capable of trimming with little change to the state of the vehicle by replacing control of the locked servo with control of rotor speed. This strategy can be used to maintain trim over 6 – 12% of the total servo ranges. At forward flight speeds, each of the three actuators produces a different result on the trimmed aircraft due to the non-axisymmetry of the rotor. Reconfiguration is accomplished through use of the ailerons, stabilator pitch, wings, and wing-mounted propellers to trim rotor produced roll moments, pitch moments, lift, and drag, respectively. The additional effectors in forward flight increases the range of tolerable failures to 20 – 63% of the maximum actuation limits.

NOTATION

P_{rotor}	main rotor power requirement (hp)
P_{total}	total vehicle power requirement (hp)
S_{fwd}	swashplate height at 121° azimuth, prescribed by forward hydraulic actuator (in)
S_{lat}	swashplate height at 211° azimuth, prescribed by lateral hydraulic actuator (in)
S_{aft}	swashplate height at 301° azimuth, prescribed by aft hydraulic actuator (in)
T_{coll}	collective thrust from the wing-mounted propellers (lbs)
α	vehicle pitch attitude, positive nose-up (deg)
β_0	blade coning angle (deg)
β_{1c}	blade longitudinal flapping angle (deg)
β_{1s}	blade lateral flapping angle (deg)
β_{min}	minimum flapping angle about the azimuth (deg)
δ_a	differential aileron, positive produces right wing-up roll moment (deg)
δ_s	stabilator pitch (deg)
ϕ	vehicle roll attitude, positive right wing-up (deg)
θ_0	blade collective pitch at 75% span (deg)
θ_{1c}	lateral cyclic pitch (deg)
θ_{1s}	longitudinal cyclic pitch (deg)
Ω	main rotor rotational speed, counterclockwise (rad/s)

Presented at the AHS International 73rd Annual Forum & Technology Display, Fort Worth, Texas, USA, May 9–11, 2017.

INTRODUCTION

Between 1984 and 1993, the United States Air Force conducted a series of tests under the Self-Repairing Flight Control System Program (SRFCS) to produce a method by which fixed-wing aircraft with enough surplus control surfaces and available power could maintain trimmed flight despite failure or loss of a control surface (Refs. 1, 2). In this study an F-16 was flown at speeds of up to Mach 0.7 while simulating one stabilator locked at a range of angles, or missing sections of its aerodynamic surface. The self-repairing system was able to reconfigure the control system, utilizing the remaining controls to re-establish full controllability of the aircraft. Similar research has been conducted since then (Ref. 3), including the Reconfigurable Control for Tailless Fighter Aircraft (RESTORE) which was sponsored by the United States Air Force in 1998, and used the experimental X-36 as a test-bed (Ref. 4). RESTORE demonstrated the capabilities of a neural network to reconfigure the aircraft control laws to improve upon the baseline control laws after simulated actuator failures locked an unknown control effector in place.

While reconfiguration after control failure is a widely explored subject for fixed-wing aircraft, limited research has been conducted in parallel for application to helicopters. Ref. 5 explores the possibility of reconfiguration in hover for a rotor with two independent servo-flaps on each blade, demonstrating that fault detection and reconfiguration strategies developed for fixed-wing aircraft can be applied if the requi-

site sensor and control redundancies exist. Ref. 6 describes a swashplate geometry that couples control axes of the main rotor actuators, and demonstrates reconfiguration after failure with a PID and a neural network based controller with main rotor speed and longitudinal flight speed as controls. Paramount to both of these studies is a manufactured level of control redundancy that is capable of tolerating conventional control failure that does not exist in a typical conventional helicopter. In Ref. 7, Hess postulates that this lack of redundant control effectors present on a conventional helicopter is why reconfiguration after failure is such a limited research subject for rotorcraft.

In a fully compounded helicopter, main rotor RPM, collective propeller thrust, differential aileron deflections, and horizontal stabilator pitch can be available as redundant control effectors. These additional controls allow for an infinite number of potential trim states to exist, which can be used to elicit any number of potential benefits including reduced power, vibrations, blade loads, and acoustic noise (Refs. 8–16). Handling qualities in maneuvering flight have also been shown to benefit from the use of additional controls (Ref. 17).

The primary goal of this paper is to explore the potential for using the redundant controls on a compound helicopter to maintain steady level flight in the event of reduced effectiveness or failure of a main rotor control. The study also develops a physical understanding of the mechanisms by which a compound helicopter may be suited to respond to these failures.

COMPOUND HELICOPTER MODELING AND ANALYSIS

The compound helicopter model used in the simulations of this study is adapted from a UH-60A rotor and fuselage model, and is very similar to the model used in Ref. 13. A schematic of the model is shown in Figure 1. Table 1 provides a detailed summary of the compound configuration's major subsystems and their characteristics. The configuration is designed for high speed flight, and the model used is representative of that. Propellers are used to provide thrust in high-speed flight, so the forward shaft tilt present on the UH-60A is removed. Furthermore, the UH-60A twist provides excellent hover performance, but the large non-linear twist rate results in high negative lift and drag at the advancing blade tips for high advance ratios, so a more moderate $-8°$ twist is considered in this study. Other features of the UH-60A rotor including airfoil selections, chord distribution, and sectional mass and stiffness properties are left unchanged. The airfoil aerodynamic coefficients are interpolated from non-linear lookup tables.

The gross takeoff weight is increased to 20,110 lbs, which is equivalent to the takeoff weight of the Piasecki X-49A SpeedHawk. This increased weight can be assumed to include the weight of the wings, propellers, and any additional weight required to compound the UH-60A airframe. To model fuselage drag, the compounded fuselage is assumed to be more streamlined than the UH-60A fuselage. A UH-60A has a minimum

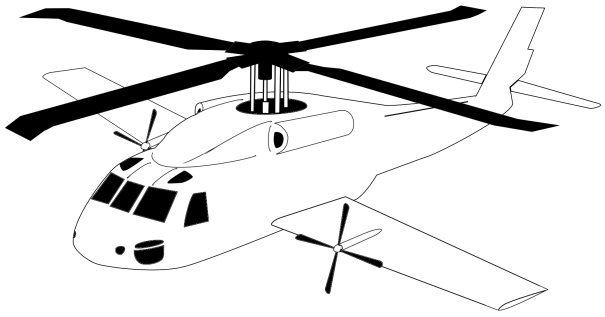

Fig. 1. Compound helicopter schematic

equivalent flat plate drag area of 35.14 ft^2 (Ref. 18). According to trends established by Ormiston (Ref. 19), a modern aircraft at this gross weight that is designed for high speed flight can be expected to have an equivalent flat plate drag area of 18.49 ft^2. The quadratic relation between vehicle pitch attitude and drag as measured for the UH-60A was maintained, resulting in the following expression for the equivalent flat plate drag area as a function of vehicle pitch attitude (in degrees).

$$f_D = 18.487 + 0.0441\alpha^2 \text{ (ft}^2\text{)}$$

The wing model is based on the three dimensional lift, drag, and moment coefficients for the wing of the Aerostar FJ-100, which is the wing used on the X-49A. For the purpose of the study in Ref. 13, it has been set at an incidence of 3.8°, so that for pitch-level flight at 225 kts it will be flying close its peak L/D of 22.4, and scaled in area from 178.2 ft^2 to 220 ft^2 so that at this attitude it will be lifting about 83% of the gross weight of the aircraft. With only 1.2° of nose-up vehicle pitch, the wings can produce enough aerodynamic lift to completely offset the aircraft weight, and will still be operating at an L/D of 21.2. Interference between the wing and rotor is not modeled in this study. In a similar study by Moodie and Yeo, interference effects were shown to increase the total power by less than 1% (Ref. 20). The effects of aileron deflections are included in the aerodynamic coefficient tables for the Aerostar FJ-100 wing for up to 10°of differential.

The propeller thrust is modeled as a point force (parallel to the waterline of the aircraft) and a yaw moment (parallel to the rotor torque vector), which are applied in line with the vertical coordinate of the center of gravity, and at the quarter-chord of the wings longitudinally. This is done so that the collective propeller thrust acts only in the longitudinal body direction without producing a coupled pitching moment. The magnitude of the thrust and the yaw moment are directly prescribed as controls. Propeller power is determined in post processing using a blade element vortex theory (BEVT) model of two pitch controlled four-bladed propellers with a 4.5 ft radius at 1,934 RPM.

The horizontal stabilizer is modeled after the size and location of the UH-60A stabilizer, with airfoil coefficients interpolated from a table of NACA 0012 wind tunnel data. Interference

Table 1. Compound helicopter configuration

Characteristic	Measurement
Gross Weight	20,110 lbs
C.G. Location	1.5 ft aft, 5.8 ft below hub
Main Rotor	
Rotor Radius	26.8 ft
Nominal Rotor Speed	258 RPM
Nominal Blade Twist	$-8°$
Shaft Tilt	$0°$
Airfoils	SC-1094 R8/SC-1095
Horizontal Stabilizer	
Effective Area	43 ft^2
Airfoil	NACA 0012
Wing	
Planform Area	220 ft^2
Chord	5 ft
Span	44 ft
Incidence Angle	3.8°
Aerodynamic Properties	Aerostar FJ-100
C.P. Location	0.5 ft aft, 6.5 ft below hub
Auxiliary Propellers	
Radii	4.5 ft
Speed	1,934 RPM
Solidity	0.12
Locations	10 ft laterally, on each wing

between the wake of the rotor and the horizontal tail is neglected.

To simulate the inflow in hover, a 12×12 Peters-He dynamic inflow model is implemented (Ref. 21). A dual core prescribed wake model is selected to model the inflow in forward flight, which captures the effects of producing negative lift on the advancing tip of the blade.

The simulations are produced using the US Army's Rotorcraft Comprehensive Analysis System (RCAS), version 15.09 (Ref. 22). The structural and aerodynamic models are built to the above mentioned specifications in RCAS using 13 elastic beam elements, 36 aerodynamic sections, and an azimuthal resolution of 5° for calculation of airloads. The flap and lag hinges, and pitch bearings are modeled as torsional spring/damper elements, and pitch control is prescribed through a spring element with a stiffness that is representative of the pitch link and swashplate stiffness of a UH-60A. As a computational tool, the RCAS UH-60A structural model has been validated against UH-60A flight test data (Ref. 23), and the prescribed wake model has been validated against wind tunnel test data of an untwisted H-34 rotor at advance ratios up to 0.46 (Ref. 24).

SWASHPLATE ACTUATORS

Actuator Geometry

The RCAS model transfers the pilot control to the blade pitch through direct control of the pitch link height. Collective, lateral and longitudinal blade pitches ($\theta_0, \theta_{1c}, \theta_{1s}$) are prescribed by displacing of the base of the pitchlink from the reference plane of the level swashplate. On the UH-60, the pitch links are attached to a rotating ring outboard of the non-rotating swashplate, shown in Figure 2. The non-rotating swashplate is positioned by three actuators ($S_{fwd}, S_{lat}, S_{aft}$), which transmit pilot control to the swashplate through a set of mechanical linkages (Refs. 25, 26). Each actuator consists of two parallel hydraulic servos to provide direct control redundancy at the expense of added weight and complexity.

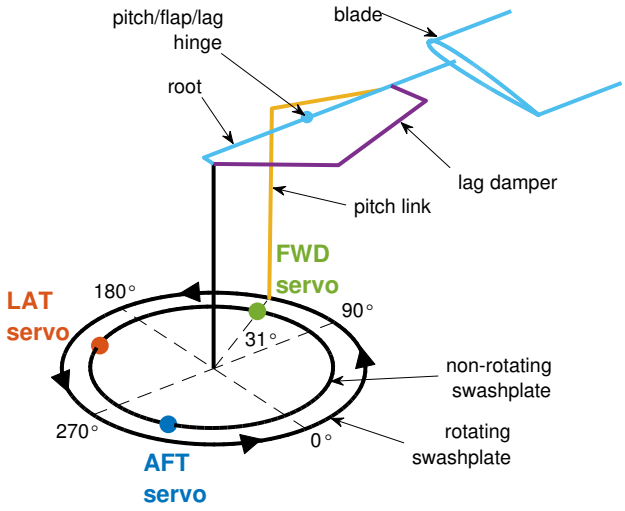

Fig. 2. Rotor hub model of a single blade at 90°azimuth with servo locations labeled

For this study the forward, lateral, and aft servos are assumed to act directly at 121°, 211°, 301°, respectively, as can be seen in Figure 2. The connection between the pitch link and the rotating swashplate leads each blade by 31°, therefore, each of the three servos effectively controls the pitch link displacement when a blade is at 90°, 180°, and 270° azimuth. It is also assumed that the actuator connections are at the same radial position as the pitch link connections, to prevent coupling. The redundant hydraulic servo in each actuator will be treated as a single servo for the sake of examining the consequences of a failure.

An RCAS trim solution, which provides controls in terms of pitch link height, can undergo a change of basis to be put in terms of servo actuation height. For the assumed geometry, the approximate relationships between blade pitches and actuator heights are given in Equations 1 – 6. To produce an increase in collective pitch without changing the cyclic pitch, all three actuators are be raised the same amount. Isolated increases longitudinal pitch results from a differential between the forward and aft actuators, while isolated lateral pitch variation is accomplished by the lateral actuator.

$$S_{fwd} \propto \theta_0 + \theta_{1s} \tag{1}$$

$$S_{lat} \propto \theta_0 - \theta_{1c} \tag{2}$$

$$S_{aft} \propto \theta_0 - \theta_{1s} \tag{3}$$

$$\theta_0 \propto \frac{(S_{fwd} + S_{aft})}{2} \tag{4}$$

$$\theta_{1c} \propto \frac{(S_{fwd} + S_{aft})}{2} - S_{lat} \tag{5}$$

$$\theta_{1s} \propto \frac{(S_{fwd} - S_{aft})}{2} \tag{6}$$

The servo naming convention is given relative to the primary effect that each actuator has on the flapping of the rotor. Increases in the forward actuator height will increase longitudinal cyclic pitch and the rotor will flap up in the front, increases in the lateral actuator height will increase lateral cyclic pitch and lateral blade flapping, and increases in the aft actuator height will reduce longitudinal cyclic pitch and produce a higher flapping angle in the rear.

Servo Failure

Ref. 26 explains two common modes of failure for the hydraulic servos. A breach of the hydraulic chamber would cause pressure loss to the actuator and result in a floating piston position as dictated by the rotor dynamics. The second failure type involves a jam of the piston within the cylinder such that the servo actuation displacement is fixed—and is the failure mode that will be considered in this study. Under this failure mode, one of the servo lengths in Equations 4 – 6 would become a constant, and result in two servo inputs controlling three pitch link outputs.

Figure 3 shows the resulting change in controllability of the main rotor. The gray box shows the control space of the main rotor under normal operating conditions, with limits given in accordance with Table 2. The blue and red planes show the reduced controllability for two sample failure states of the lateral actuator, at 0" and 2", respectively. Pure control of the longitudinal cyclic pitch is still possible when constrained to one of these planes, since differential between the forward and aft servos is not affected by the lateral servo. However, increase in lateral cyclic pitch (θ_{1c}) cannot be accomplished without a coupled increase in collective pitch (θ_0), and is accomplished by raising the forward and aft servos relative to the lateral servo (Eqn. 5). Despite having lost full controllability of the main rotor, it may still be possible to maintain trim through use of the additional controls.

SERVO FAILURE IN HOVER

For the compound helicopter in hover, main rotor speed, and collective propeller thrust are the two additional controls that are capable of affecting the trim of the aircraft (since wake interactions with other aerodynamic control surfaces are neglected). Trim solutions are produced in RCAS through parametric variations in collective propeller thrust (from $-3,500$ to $3,500$ lbs in 500 lbs increments) and in rotor speed (from 21 to 27 rad/s in 1 rad/s increments). A total of 74 trim states were found that satisfy trim in addition to the constraints listed in Table 2.

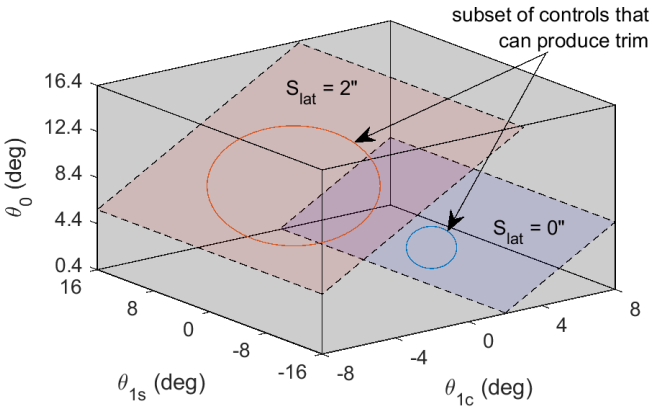

Fig. 3. Visualization of 3-D space of main rotor control, with two planes showing sub-spaces of rotor control with impinged S_{lat}

Table 2. UH-60A main rotor control and flapping limits

Rotor Condition	Limits
Collective Pitch	$0.4° \leq \theta_0 \leq 16.4°$
Lateral Cyclic Pitch	$-8° \leq \theta_{1c} \leq 8°$
Longitudinal Cyclic Pitch	$-16° \leq \theta_{1s} \leq 16°$
Blade Flapping Angle	$-6° \leq \beta \leq 22°$
Adv. Tip Mach No.	$M_{tip} \leq 0.89$

The changes to trim induced by variation in the compound controls also produce variations in the conventional trim variables, which translate to the swashplate actuators. For each plot in Figure 4 the total vehicle power requirement is plotted as a function of one of the three servo positions. Each point on the plot represents one of the parametric sweep trim solutions, and is colored by the main rotor speed.

The two degrees of redundancy allow for an infinite number of possible trim states, even after constraining an actuator to a fixed height. Any vertical slice of constant actuator from Figure 4 could be represented as a plane of reduced subspace as in Figure 3. On each of these planes, a circled region represents the intersection between the subset of controls which can be used to produce a trim solution, and the subset of controls that are attainable with the locked actuator.

The black line in Figure 4 marks the Pareto front for minimum power, and is the most efficient combination of controls that produce trim for each value of actuator height along the x-axes. The change in actuator heights that occurs while moving along the Pareto fronts are shown in Figure 5, and the resultant blade pitches are shown in Figure 6.

With full control availability, a minimum power state exists at a rotor speed of about 23 rad/s. This minimum exists between the profile power dominated region at higher rotor speeds and the induced power dominated region at lower rotor speeds. Trim state A, however operates at the nominal rotor speed for the UH-60A (27 rad/s), and is thus is chosen as a baseline. Table 3 provides details on this, and the other trim states marked along the Pareto front in Figure 4. If the piston of a servo were to become impinged while aircraft is in some flight con-

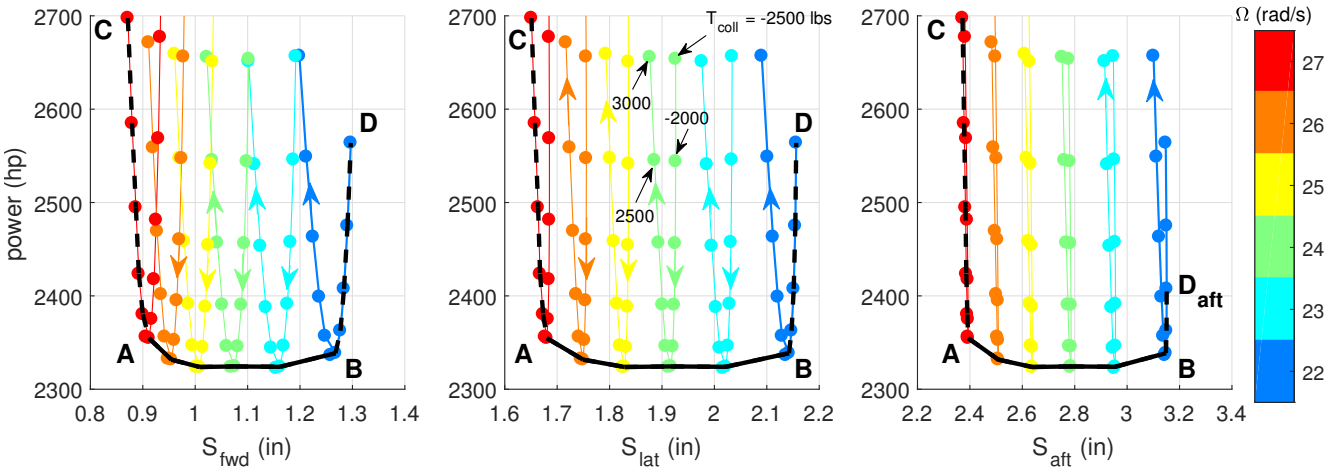

Fig. 4. Variation of trim state power (hp) due to servo position, and colored by rotor speed (rad/s) in hover, with arrows denoting direction of increasing auxiliary thrust

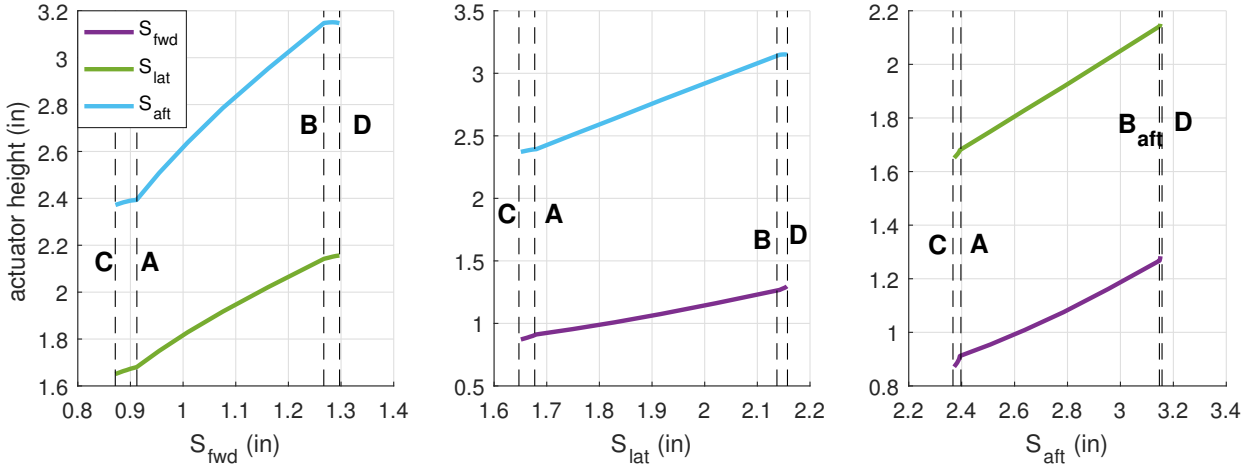

Fig. 5. Variation of remaining servos along the Pareto front of minimum power for a fixed servo in hover

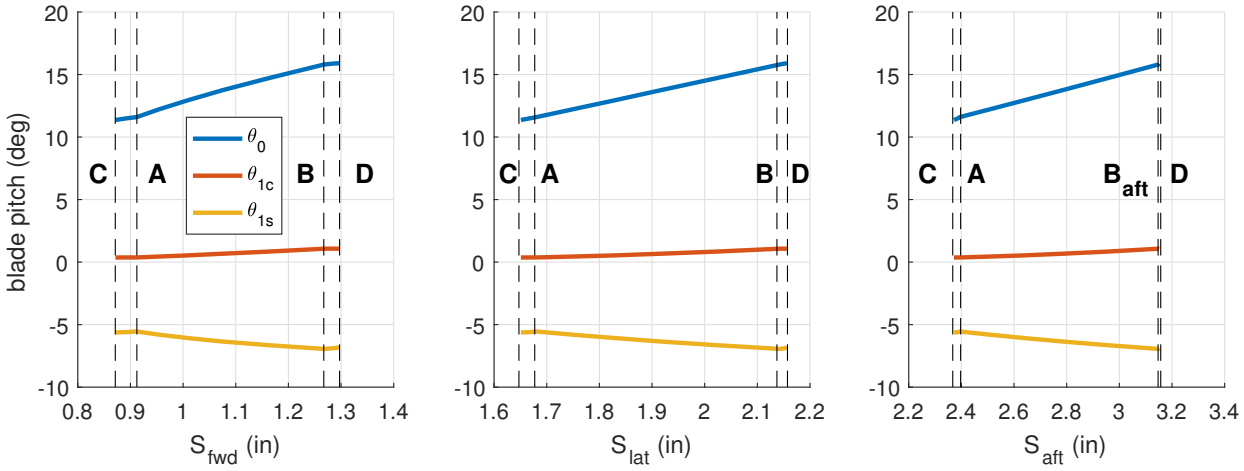

Fig. 6. Resultant blade pitches along the Pareto front of minimum power for a fixed servo in hover

dition other than steady hover (at a different velocity, altitude, gross weight, or through a maneuver), the forward actuator is likely to be in a position other than the 0.91" height required of trim state A. To this end, the states on either limit of the Pareto fronts demonstrate the range of locked actuator heights for which the aircraft can maintain trim.

Table 3. Trimmed Pareto front limits in hover

	A	B	C	D
S_{fwd}	0.91"	1.27"	0.87"	1.30"
S_{lat}	1.68"	2.14"	1.65"	2.16"
S_{aft}	2.39"	3.15"	2.37"	3.15"
θ_0	11.6°	15.8°	11.4°	15.9°
θ_{1c}	0.4°	1.1°	0.4°	1.1°
θ_{1s}	−5.5°	−6.9°	−5.6°	−6.8°
Ω	27 rad/s	22 rad/s	27 rad/s	22 rad/s
T	0 lbs	0 lbs	3,000 lbs	−2,000 lbs
ϕ	0.1°	0.4°	0°	0.4°
α	5.8°	7.3°	14.5°	1.5°
β_0	3.8°	6.0°	3.7°	6.0°
β_{1c}	5.4°	6.7°	5.5°	6.6°
β_{1s}	−0.4°	−0.7°	−0.4°	−0.7°
P_{total}	2,355 hp	2,339 hp	2,698 hp	2,564 hp
Main Rotor Thrust (lbs)				
Up	20,027	20,025	19,276	20,078
Fwd	0	0	−2,906	1,998
Auxiliary Thrust (lbs)				
Up	0	0	750	−54
Fwd	0	0	2,905	−1,999

Due to the near axisymmetry of the rotor in hover, the method of compensation for failure is approximately the same for each of the servos, therefore only the forward servo (S_{fwd}) will be examined in detail. As S_{fwd} increases along the Pareto front from trim state A to state B (0.91" to 1.27"), the main rotor speed decreases, but according to Table 3, there is no significant change in the collective propeller thrust (to the nearest 500 lbs). During this variation, the remaining actuators adjust as seen in Figure 5, so that lateral and longitudinal cyclic pitches only increase by 0.7° and −1.3°, respectively. Collective pitch absorbs most of the actuator variation, increasing by 4.2°. Each of these pitch increases are prevented from significantly increasing the rotor thrust due to the reduction of rotor speed and the dynamic pressures on the blades. From the actuators' lowest height to their highest height, the combined effects of higher blade pitch and lower rotor speeds results in a reduction of the net rotor thrust by only 2 lbs (Table 3). Changes to pitch and roll moments about the aircraft center of gravity are negligible. The only significant change to the rotor moments comes in the form of torque, which is counteracted by differential propeller thrust.

In this manner, the length of actuator variation between trim state A and B is capable of using the main rotor speed as a redundant main rotor control, with minimal changes to the rest of the aircraft operating state. This range is bounded on the upper limit by collective pitch, which is constrained to a maximum value of 16° (from Table 2), and on the lower limit by rotor speed, which is constrained to the maximum nominal value of 27 rad/s. Further actuator travel can be achieved through introduction of thrust variation, along the dashed segments of the Pareto fronts in Figure 4. For S_{fwd}, this moves the lower limit from state A to C, and the upper limit from state B to D.

Moving from trim state B to D keeps main rotor speed constant at its lower limit, while collective propeller thrust becomes increasingly negative. The collective propeller thrust produces a net backwards thrust on the vehicle that causes the main rotor to trim with a larger opposing forward thrust, which comes from trimming at a slightly more nose level pitch, while increasing the collective pitch and longitudinal cyclic pitch of the rotor. As shown in Eqn. 1, S_{Fwd} is maximized as collective and longitudinal pitches increase, therefore the increased negative collective propeller thrust at trim state D raises the swashplate and extends the actuator by an additional 0.03".

Relative to S_{fwd} and S_{lat}, this effect is less pronounced for S_{aft}, as can be observed by the lack of any added range between states B and D. The parabolic trajectory of increasing collective propeller thrust in Figure 4 is most narrow for S_{aft}, demonstrating a reduced correlation between actuation and collective propeller thrust in trim. The more positive collective and longitudinal pitches that were added together in Eqns. 1 to give the height of S_{fwd} are subtracted from each other in Eqn. 3 to give the height of S_{aft}. The increase in collective pitch raises S_{aft}, but the increased longitudinal cyclic pitch lowers it by about the same amount. S_{lat} only increases by "0.02", as it benefits from the raised collective pitch, but is unaffected by changes in longitudinal cyclic pitch, and the lateral cyclic pitch remains constant (Eqn. 2).

On the lower end of the Pareto front, the opposite control variations are observed. At trim state C, the collective propeller thrust has increased positively to 3,000 lbs, while the main rotor speed is preserved at 27 rad/s. Consequently, the collective pitch is reduced 0.2° from trim state A, while the vehicle pitches up to an attitude of 14.5°, to position 2,906 lbs of the main rotor thrust in opposition to the propeller thrust. The reduction in collective pitch is feasible because of the 750 lbs of the propeller thrust positioned in the vertical direction by the nose up pitch attitude. Table 3 shows longitudinal pitch is reduced by 0.1°. The net reduction in blade pitches contribute to a 0.02"–0.04" reduction in each of the three actuator heights relative to trim state A.

Relative to the 0.36" in S_{fwd} variation achievable through pure rotor speed variation, collective propeller thrust only adds up to an additional 19% of actuator range at the cost of a 10–15% increase to power. For S_{lat} and S_{aft} the same cost in power give diminished increases to the range of actuator heights (11% and 3%, respectively). While extending the range of actuator position with propeller thrust may be possible when further exercising of rotor speed isn't, the benefits are very limited at a cost of high power.

SERVO FAILURE AT 100 KTS

With a non-zero free stream velocity, dynamic pressure on the wings and tail allows use of two additional control effectors—differential aileron and stabilator pitch. To accommodate the larger envelope of possible trim states, the parametric sweeps were adjusted for collective propeller thrust (from 0 to 6,000 lbs in 500 lbs increments) and rotor speed (from 17 to 27 rad/s in 1 rad/s increments), and additional sweeps were performed in stabilator pitch (from $-18°$ to $18°$ in $3°$ increments) and aileron differential pitch (from $-10°$ to $10°$ in $5°$ increments). Many of these cases were unable to converge, or resulted in infeasible trim solutions subject to the constraints in Table 2, but a total of 3,020 feasible trim solutions were found and plotted in Figure 7. As with hover, each point is colored by the main rotor speed used to generate each flight state, and a Pareto front is created by the minimum power trim states for a range of servo actuation heights.

Contrary to what was observed in hover, there is almost no correlation between rotor speed and actuator position along the Pareto front. Rather, variation in rotor speed is more closely correlated to increasing power requirement. Stronger correlations exist between actuator positions and the remaining three controls: collective propeller thrust, stabilator pitch, and differential aileron deflections in Figures 8, 9, and 10, respectively. Detailed examinations of the effect of variation in each actuator along the Pareto front are presented in the following sections. Trim state A is selected as the baseline case, as it is a common point on all three Pareto fronts and is the minimum power state for 100 kts. Relevant details on every point marked on Figures 7 – 10 are provided in Table 4.

At trim state A, 27% of the lift is being generated by the wing, and 67% is being generated by the rotor, with the fuselage and stabilator lift accounting for the remaining 683 lbs of lift. The main rotor operates with a speed of 22 rad/s (81% of nominal), and is trimmed with the rotor flapping slightly forward such that it is effectively drag-neutral—producing neither a net drag force, nor a propulsive thrust. The main rotor power requirement is only 421 hp, with the remaining 364 hp of the total power requirement being used to generate 1,000 lbs of collective thrust from the propellers to overcome the vehicle's drag (which is reduced relative to the baseline UH-60A).

Forward Actuator

To show the strategies used to trim while allowing high S_{fwd} actuation, the nominal trim state (A) will be compared to the upper end of the Pareto front boundary, trim state B_{fwd}. From A to B_{fwd}, S_{fwd} has increased from -0.08" to 1.20". Figure 11 shows how S_{aft} and S_{lat} respond to increasing S_{fwd} along the Pareto front, to give the main rotor controls in Figure 12. Trim state B_{fwd} allows this 1.28" increase in S_{fwd} by reducing S_{aft} by 1.63", which combines to give a $11.2°$ increase in longitudinal pitch and a $1.3°$ reduction in collective pitch—as described by the relationships given in Eqns. 4 and 6. The 0.36" reduction in S_{lat} is used to keep lateral cyclic pitch constant irrespective of the changes in the other two actuators (Eqn. 5). At trim state A, the $-10.0°$ of longitudinal pitch was used to counteract the natural tendency of a rotor to flap backwards in forward flight, and helps produce its drag-neutral rotor state. Increasing this longitudinal pitch to $1.2°$ at trim state B_{fwd} causes the main rotor to blow back, with a longitudinal flapping angle of $-5.1°$ relative to the $5.2°$ of forward flapping at trim state A.

These changes in the main rotor state produce system-level changes in rotor force and moment production, which can be equilibrated by the additional control effectors to maintain a steady flight condition. The blow-back of the rotor generates an up-wash through the disk from the free-stream velocity, which increases rotor lift and drag. The 2,389 lbs of added rotor lift requires an offloading of the wing from a 24% lift share to a 10% lift share, so the trimmed vehicle pitch attitude is reduced from $5.1°$ to $-1.5°$. The 1,210 lbs of increased rotor drag are trimmed by a doubling of the collective propeller thrust from 1,000 lbs to 2,000 lbs. Because of its location above the center of gravity, the increased rotor drag also produces a large nose-up pitch moment, which requires an opposing nose-down pitching moment from the stabilator. The stabilator pitch is increased accordingly by $18°$. After accounting for the $6.6°$ reduction in vehicle pitch attitude, the net result is a $11.4°$ increase in stabilator angle of attack, to produce a large increase in nose-down pitch moment. For very high stabilator pitches of $15°$ – $18°$, some states in Figure 9 exhibit a reduction in S_{fwd} and a power increase, which is due to stalling of the stabilator. Stabilator stall is therefore the active constraint limiting further extension of S_{fwd} by this strategy.

The S_{fwd} minimum allowable trim state is labeled C_{fwd} on the Pareto fronts in Figures 9 – 10 and in Table 4. From Figure 11 the 0.26" reduction in S_{fwd} from the baseline at trim state A is accompanied by increases in S_{lat} and S_{aft}. This combination of servo actuators produces a net $4.7°$ reduction in longitudinal pitch and $1.0°$ increase in collective pitch shown in 12. The primary result is a highly negative $-14.7°$ of longitudinal cyclic pitch and a forward flapping angle ($9.5°$).

At trim state C_{fwd}, the forward tilt of the main rotor positions a 631 lbs of the rotor thrust acting in the propulsive direction, which produces a coupled effect of a nose-down pitch moment, and a reduction in the main rotor thrust acting to produce lift. These are counteracted by the stabilator pitch, which is reduced from $-3°$ to $-9°$, and the collective propeller thrust, which is reduced from 1,000 lbs to 500 lbs. Additionally, the vehicle pitch attitude has increased to $7.0°$, and the wing lift share has increased to 32% as the rotor lift reduces. With the vehicle at a high pitch attitude and an offloaded rotor with low coning and high forward flapping, the rotor flapping can become excessively negative. The lower bound of S_{fwd} is limited by the main rotor droop stop, which prevents excessively negative flapping angles of $-6°$ or larger.

From the lowest value of S_{fwd} at trim state C_{fwd} to the upper limit at B_{fwd}, the actuator height varies from -0.53" to 1.20". Increasing S_{fwd} along the minimum power boundary shows that the remaining servos are best utilized to increase

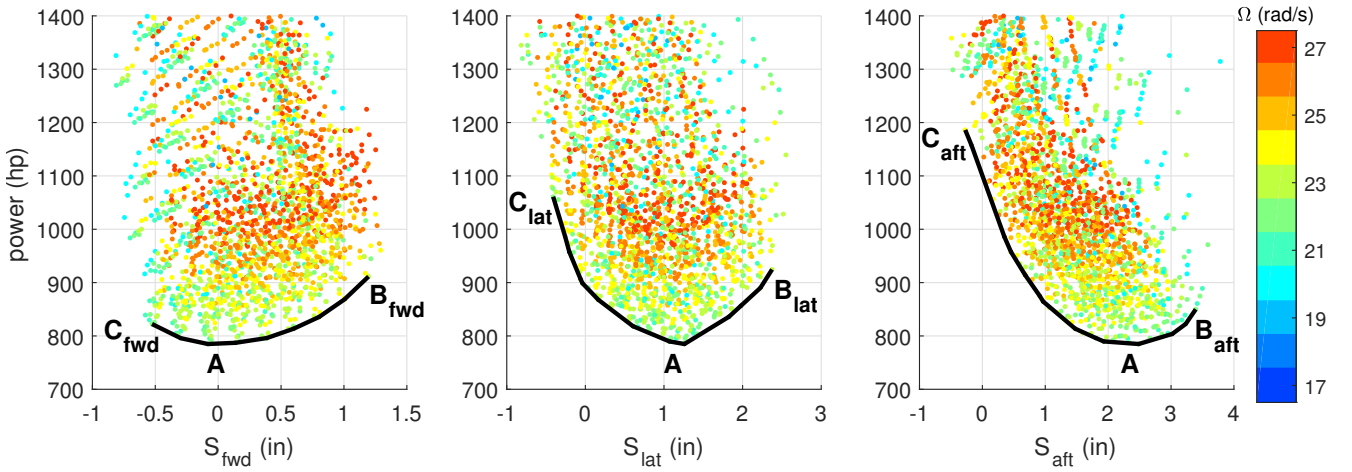

Fig. 7. Variation of trim state power (hp) due to servo position, and colored by rotor speed (rad/s) at 100 kts

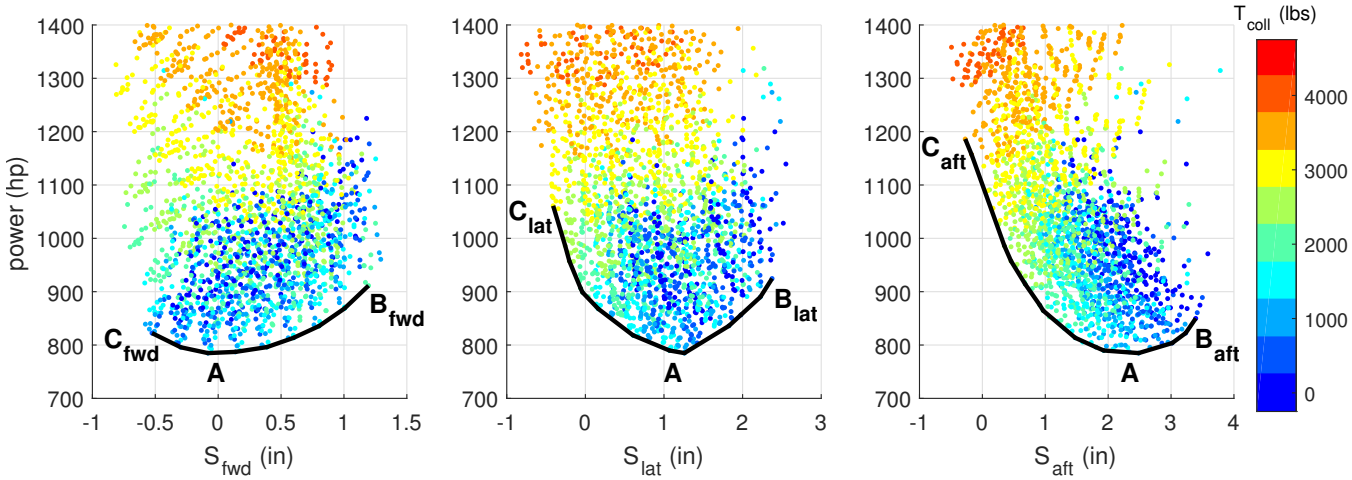

Fig. 8. Variation of trim state power (hp) due to servo position, and colored by collective auxiliary thrust (lbs) at 100 kts

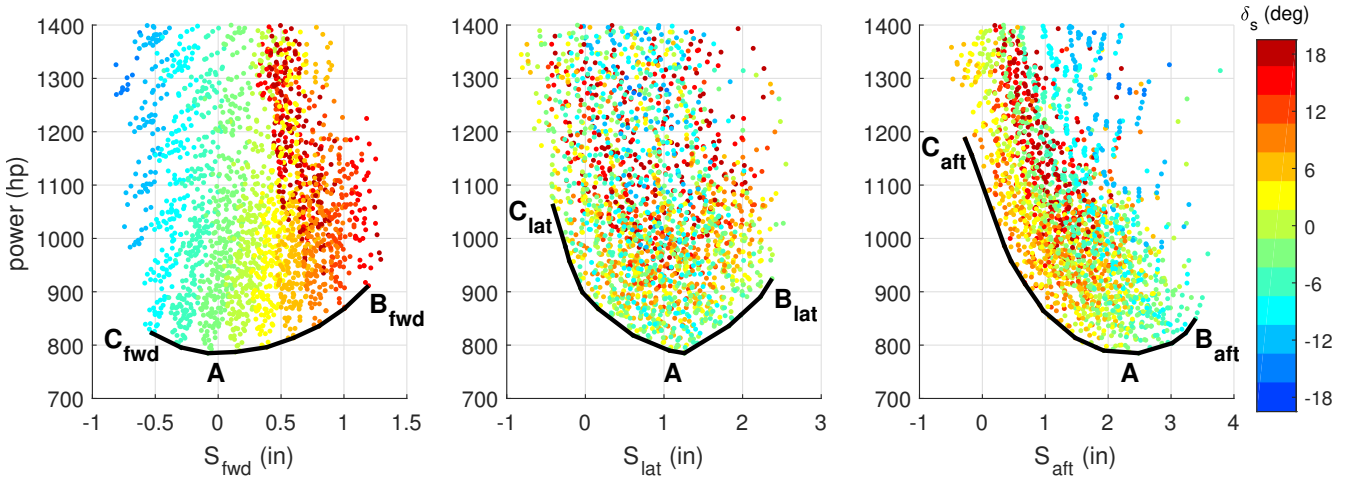

Fig. 9. Variation of trim state power (hp) due to servo position, and colored by stabilator pitch (°) at 100 kts

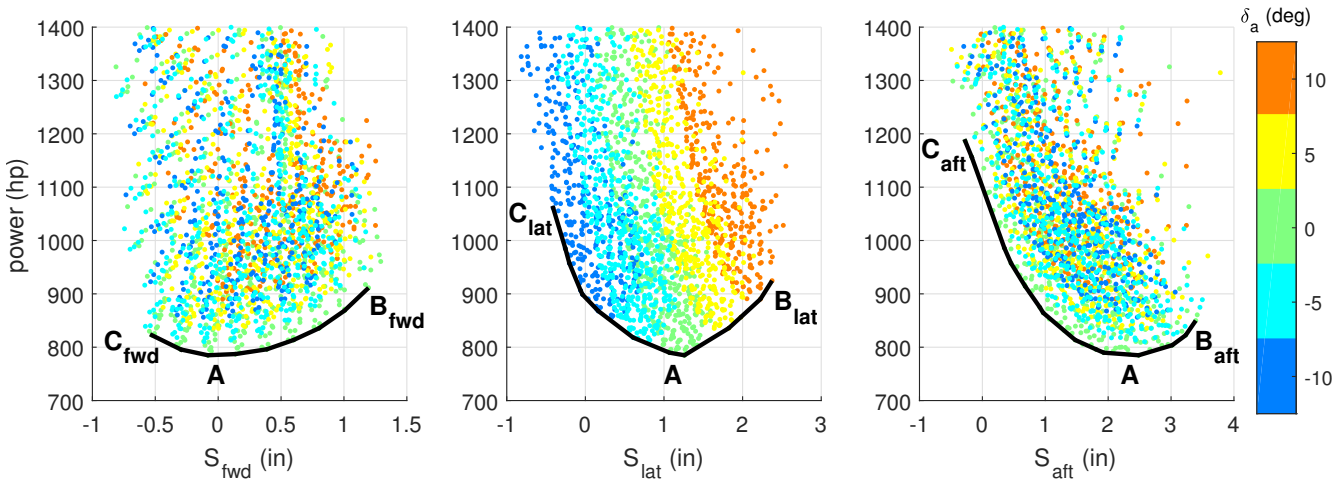

Fig. 10. Variation of trim state power (hp) due to servo position, and colored by differential aileron (°) at 100 kts

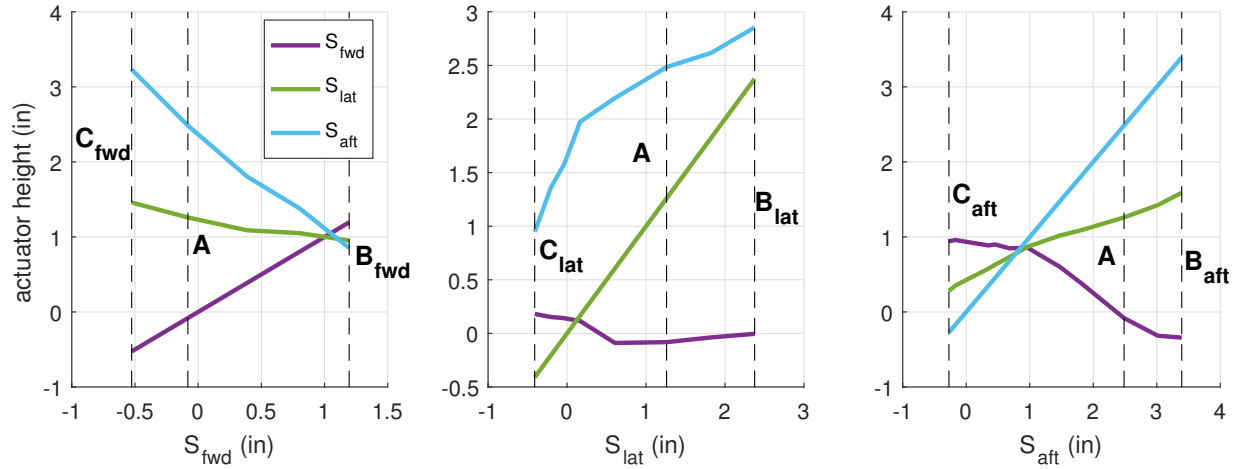

Fig. 11. Variation of remaining servos along the Pareto front of minimum power for a fixed servo at 100 kts

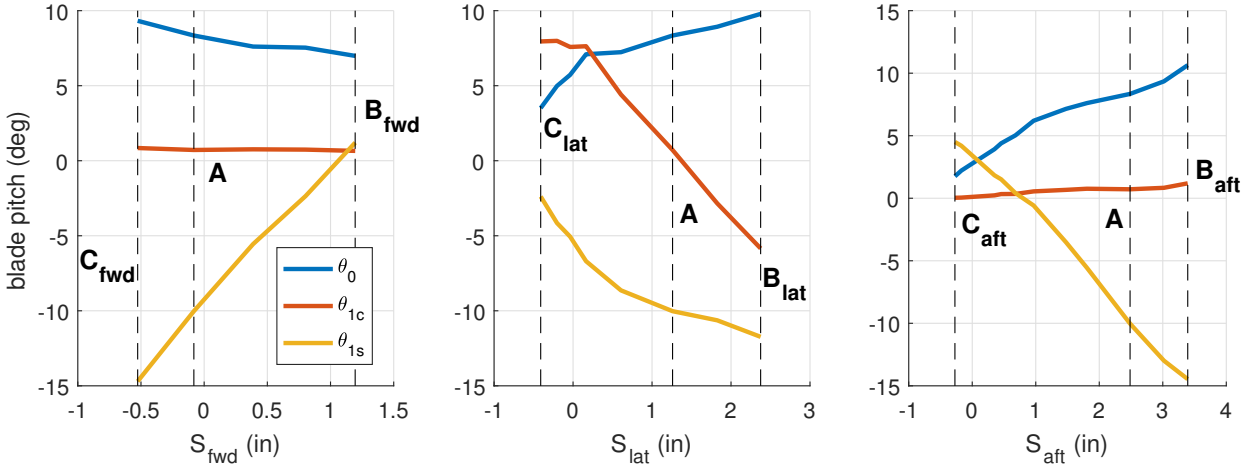

Fig. 12. Resultant blade pitches along the Pareto front of minimum power for a fixed servo at 100 kts

Table 4. Trimmed Pareto front limits at 100 kts

	A	B_{fwd}	B_{lat}	B_{aft}	C_{fwd}	C_{lat}	C_{aft}
S_{fwd}	−0.08”	**1.20”**	0.00”	−0.34”	**−0.53”**	0.18”	0.94”
S_{lat}	1.26”	0.95”	**2.38”**	1.59”	1.46”	**−0.41”**	0.28”
S_{aft}	2.48”	0.85”	2.85”	**3.39”**	3.23”	0.95”	**−0.27”**
θ_0	8.3°	7.0°	9.8°	10.6°	9.3°	3.5°	1.8°
θ_{1c}	0.7°	0.7°	−5.8°	1.2°	0.8°	7.9°	0.0°
θ_{1s}	−10.0°	1.2°	−11.7°	−14.5°	−14.7°	−2.4°	4.5°
Ω	22 rad/s	23 rad/s	23 rad/s	22 rad/s	22 rad/s	22 rad/s	24 rad/s
T_{coll}	1,000 lbs	2,000 lbs	500 lbs	0 lbs	500 lbs	3,000 lbs	3,500 lbs
δ_s	−3°	15°	3°	−6°	−9°	0°	9°
δ_a	0°	0°	10°	0°	0°	−10°	0°
ϕ	0.1°	0°	−5.6°	0.1°	0.1°	5.4°	−0.2°
α	5.1°	−1.5°	4.3°	4.9°	7.0°	7.1°	4.5°
β_0	3.8°	4.1°	4.0°	4.1°	3.7°	3.2°	2.6°
β_{1c}	5.2°	−5.1°	5.8°	8.4°	9.5°	−0.4°	−5.8°
β_{1s}	−1.0°	−1.0°	−7.8°	−1.2°	−1.1°	6.7°	−1.2°
β_{min}	−1.5°	−1.1°	−5.7°	−4.4°	−5.8°	−3.4°	−3.3°
P_{rotor}	421 hp	166 hp	727 hp	801 hp	625 hp	−133 hp	−257 hp
P_{total}	785 hp	911 hp	925 hp	850 hp	822 hp	1,061 hp	1,186 hp
Main Rotor Forces and Moments (lbs) or (lbs-ft)							
Lift	13,943	16,332	15,576	14,548	13,551	12,858	12,624
Drag	10	1,220	−498	−976	−631	1,814	2,505
Pitch Mom.	1,627	45,640	735	−10,654	−14,844	20,754	42,973
Roll Mom.	−945	105	−28,547	−1,751	−1,941	27,528	471
Wing Forces and Moments (lbs) or (lbs-ft)							
Lift	5,484	2,160	4,066	5,402	6,348	5,487	5,197
Roll Mom.	−1	0	27,205	0	−1	−27,377	1
Stabilator Moments (lbs-ft)							
Pitch Mom.	−8,211	−49,389	−4,823	4,106	7,586	−27,371	−49,360

the longitudinal cyclic pitch, which generates increased rotor lift, drag and nose-up pitching moments. Reconfiguration after impingement of the S_{fwd} actuator in forward flight is most directly trimmed through variation in vehicle pitch attitude, collective propeller thrust, and stabilator pitch to balance the rotor forces and moments, and is bounded by the stabilator stall margin on the upper limit and minimum flapping angle on the lower limit. This conclusion is corroborated by Figure 9, which shows a strong correlation with stabilator pitch from −9° to 15° as S_{fwd} increases from trim state C_{fwd} to B_{fwd}.

Aft Actuator

While S_{aft} affects the same pitch controls as S_{fwd}, it lies on the opposite side of the swashplate, and thus has the opposite relationship with longitudinal cyclic pitch. In Eqn. 3, S_{aft} is proportional to the difference of collective pitch less longitudinal cyclic pitch, rather than the sum of the two controls. Therefore, there are a different set of trim states, labeled B_{aft} and C_{aft} at the Pareto front limits in Figures 7 – 10. The difference between the ideal main rotor controls which produce extreme S_{fwd} and S_{aft} limits are shown Table 5. Figure 13 compares free body diagrams of the four trim states with major subsystem forces labeled, and rotor flapping and vehicle pitch attitudes to scale, and Table 4 details each of these trim states.

Table 5. Comparison of ideal main rotor controls at forward and aft actuator limits

	S_{fwd}	S_{aft}
lower limit (C)	$min\ \theta_0$ $min\ \theta_{1s}$	$min\ \theta_0$ $max\ \theta_{1s}$
upper limit (B)	$max\ \theta_0$ $max\ \theta_{1s}$	$max\ \theta_0$ $min\ \theta_{1s}$

For the main rotor, the differences in actuator positions moving from trim state C_{fwd} to B_{fwd} primarily increased the longitudinal cyclic pitch, with a slight reduction in collective pitch. While the reduction in collective pitch was necessary to prevent overproduction of drag and stall of the stabilator with rotor blow-back, it was counterproductive to increased S_{fwd} variation, as shown by Table 5. For S_{aft} in Figure 11, there is a larger 3.66” range of allowable actuation from trim state C_{aft} to B_{aft}, accompanied by an increase in S_{lat} and a reduction in S_{fwd}. Over this range, lateral cyclic pitch stays effectively constant, while collective pitch increases and longitudinal cyclic pitch decreases—reverse of the direction seen for S_{fwd}. The increased limits can be primarily attributed to the

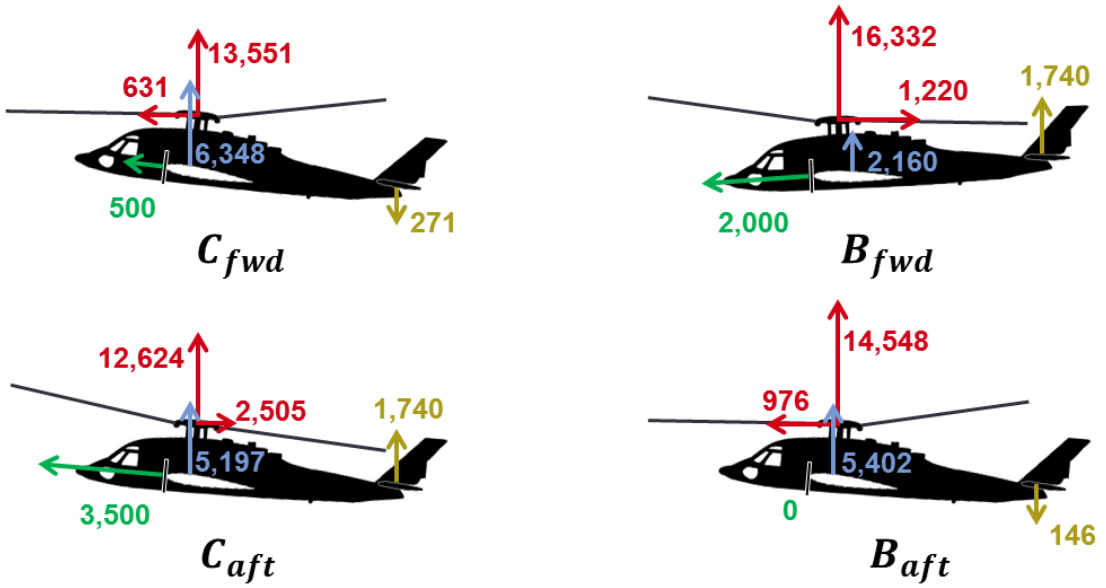

Fig. 13. Free body diagrams comparing major subsystem forces (lbs) at 100 kts (vehicle pitch attitude and blade flapping angles to scale)

increase in collective pitch, which is productive to increasing S_{aft} range.

At the maximum of S_{aft} (trim state B_{aft}), the longitudinal cyclic pitch is 0.2° lower relative to C_{fwd}, while the 1.3° higher collective pitch contributes to a greater total rotor thrust magnitude. From Figure 13, the 1,097 lbs increase in rotor thrust is trimmed in the vertical direction by a 2.1° lower vehicle pitch attitude, and 946 lbs less wing lift. Additionally, the rotor propulsive thrust component increases to 976 lbs, which is trimmed by reducing the collective propeller thrust to 0 lbs. Relative to C_{fwd}, the reorienting of the rotor thrust is accomplished from the lower vehicle pitch attitude, and the longitudinal rotor flapping is reduced by 1.1°. Consequently, the main rotor pitching moment reduces and the stabilator pitch is increased from −9° to −6° to produce less of a nose-up pitch moment. At trim state C_{fwd}, the longitudinal flapping had also resulted in a −5.8° minimum flapping angle. The lower vehicle pitch attitude and reduced longitudinal flapping in trim state B_{aft} increases the minimum flapping angle to −4.4°. With the flapping angle relaxed, the active constraint on S_{aft} travel is imposed by the minimum collective propeller thrust limit of 0 lbs.

From Table 4 and Figure 12, the S_{aft} minimum at trim state C_{aft} sets S_{aft} to −0.27" to give a collective pitch setting of 1.8° and a longitudinal cyclic pitch of 4.5°, while lateral cyclic is set to 0.0°. Relative to trim state B_{fwd}, the collective pitch is 5.2° lower, and the longitudinal pitch is 3.3° higher. With the increased −5.8° of rotor blow-back, and 4.5° vehicle pitch attitude, a large component of free-stream velocity produces up-wash through the rotor disk to reduce rotor power to −257 hp, and increase rotor drag to 2,505 lbs. The low collective pitch setting reduces the rotor lift to 12,624 lbs. The high rotor drag is trimmed by 3,500 lbs of collective propeller thrust, and the associated pitch moment is trimmed by a high 9° of stabilator pitch. Over the full actuation range of S_{aft}, the vehicle pitch attitude is much more consistent than for S_{fwd}, which reduces the necessary stabilator pitch variation.

In summary, the strategies used to compensate for S_{aft} variation is similar to S_{fwd}, but due to the relationships in Eqns. 1 and 3, some key differences arise between the two longitudinal actuators. In both B_{fwd} and C_{fwd}, the rotor used high longitudinal flapping to produce either a propulsive or drag force, while the vehicle pitch attitude was set to oppose the flapping angle, which encouraged more extreme longitudinal cyclic pitches to accomplish the necessary longitudinal force production. In trim state B_{fwd}, the high blow-back but low vehicle pitch attitude meant that a relatively high collective pitch (compared to C_{aft}) was necessary to produce sufficient rotor lift and drag. In trim state C_{fwd}, the forward flapping and high vehicle pitch attitude allowed a relatively low collective pitch (compared to B_{aft}), since the wing lift share was relatively high. To produce such large ranges in vehicle pitch attitude while maintaining similar stabilator pitches to the S_{aft} limits, an increased range of stabilator deflections were used. It is therefore most accurate to say that S_{fwd} variation is accomplished through stabilator pitch to orient the vehicle from an extreme nose-up to an extreme nose-down attitude, while collective propeller thrust varies from a low to a high setting.

In contrast, for B_{aft} and C_{aft} the rotor uses slightly less longitudinal flapping to produce either a propulsive or drag force, while the vehicle pitch attitude remains relatively stationary. The total result is a more extreme range of rotor longitudinal force, which is trimmed by a larger range of collective propeller thrust. Since the wing lift share is not significantly changing, collective pitch will simply decrease due to the upwash through the disk at trim state C_{aft}. S_{aft} variation can

thus be accomplished through collective propeller thrust variation, with stabilator pitch varied to a lesser degree relative to S_{fwd} in order to balance the pitching moment that is necessarily produced by the rotor. While correlations exist between both controls for S_{fwd} and S_{aft}, the stronger of the two is between S_{aft} and collective propeller thrust, and between S_{fwd} and stabilator pitch. The total variation allowable through these strategies produce a range of 3.66" in S_{aft}. These observations are corroborated qualitatively by Figures 8 and 9.

Lateral Actuator

From Eqns. 4 – 6, all three actuators induce changes in lateral cyclic pitch, but it is twice as sensitive to changes in S_{lat} than in S_{fwd} or S_{aft}. At trim state A the 1.26" of S_{lat} is primarily associated with the 0.7° lateral cyclic pitch, and the rotor produces $-1°$ of lateral flapping and a negligible roll moment from the retreating side. Going from trim state A to B_{lat} in Figure 11, correlates to a substantial increase in S_{lat} from 1.26" to 2.38", while the remaining two actuators increase marginally. Figure 12 shows a resulting $-6.4°$ change in lateral cyclic pitch, with a less significant 1.5° increase in collective pitch and $-1.7°$ reduction in longitudinal cyclic. The high lateral cyclic pitch increases lateral flapping to $-7.8°$, which increases the rotor roll moment from the retreating side of the rotor disk. Large roll moments are best trimmed by the ailerons, which are set to 10° to produce an opposing right wing up roll moment. With a slightly higher collective pitch and more negative longitudinal cyclic, the rotor also produces more lift, and 498 lbs of propulsive thrust. As was seen with S_{fwd} and S_{aft}, these are trimmed with a reduction in collective propeller thrust, a reduction in vehicle pitch attitude, and an increase in stabilator pitch. With 5.8° longitudinal flap and $-7.8°$ lateral flap, the minimum flap angle is $-5.7°$, and is very close to the limit. The 1 rad/s increase in rotor speed at trim state B_{lat} (from trim state A) increases the centrifugal component of flap stiffness to prevent the high cyclic pitch from producing flapping excessive enough to violate the constraint in Table 2. Trim state B_{fwd} is therefore limited by the minimum flapping constraint, as well as the limits on differential aileron deflection—which were bounded to $\pm 10°$ in this study.

In order to go from trim state A to the minimum S_{lat} height at C_{lat}, S_{lat} is reduced to -0.41" along with the other actuator variations in Figure 11. For most of the reduction, the actuators vary in a consistent manner with what was seen between A and B_{lat}. When S_{lat} is reduced to values below 0.1" in Figure 12, the lateral cyclic pitch is between 7° and 8°, and further increases cannot be tolerated by the maximum lateral cyclic pitch constraint. From Eqn. 2, S_{lat} is proportional to both collective pitch and lateral cyclic pitch, so when further lateral cyclic pitch is infeasible, a reduced S_{lat} can still be tolerated by lowering the collective pitch with constant lateral cyclic. The lowest end of the S_{lat} Pareto front is therefore accompanied by the steep reduction in S_{aft} and slight increases in S_{fwd} in Figure 11, resulting in lower collective pitches, and less negative longitudinal cyclic pitches. The main rotor produces a higher drag force as it flaps back, and the lift production is offloaded to the wings (Table 4). At the vehicle level, this is trimmed using a combination of increased vehicle pitch attitude, negative differential ailerons, stabilator pitch, and collective propeller thrust.

In summary, S_{lat} can undergo variations from -0.41" to 2.38" primarily through differential ailerons to produce internal rolling moments, which balanced those generated by the lateral cyclic pitch. From Figures 7 – 10, the greatest correlation between the four compound controls and S_{lat} variation was with the differential ailerons in Figure 10. Additionally, the other two actuators can also be used to produce collective pitch variations at the limits of lateral cyclic pitch travel to further the range of S_{lat}.

For hover, rotor speed variation was the only redundant control with the ability to produce variations in the actuation of the servos. For all three actuators at 100 kts, there is a substantially expanded lower range of actuation, which can be attributed to the addition of the remaining three controls. With the fixed systems able to produce more of the required forces and moments to trim the aircraft, the rotor is able to tolerate larger variations in forces and moments without preventing feasible trim.

SERVO FAILURE AT 200 KTS

At 200 kts the parametric sweeps were performed in collective propeller thrust (from 0 to 6,000 lbs in 500 lbs increments), main rotor speed (from 17 to 25 rad/s in 1 rad/s increments), stabilator pitch (from $-6°$ to 12° in 1.5° increments), and aileron differential pitch (from $-5°$ to 5° in 1° increments). The 391 converged, feasible trim solutions (subject to the constraints listed in Table 2) are plotted in Figures 14 – 17, with color representing variation in rotor speed, collective propeller thrust, stabilator pitch, and differential aileron pitch, respectively. A minimum power trim state, A, is again selected as the baseline case since by definition it is a common point on all three Pareto fronts at 200 kts. Relevant details on every trim state marked on Figures 14 – 19 are provided in Table 6.

At 100 kts, the most efficient trim state generated 27% of the lift from the wing, allowing the rotor to offload slightly and reduce its rotor speed for a power benefit. At trim state A with a 200 kts flight speed, this has been increased to 73% of the lift being generated by the wing, which is a much more efficient lifting body. With the main rotor offloaded, the rotor speed can be reduced to 19 rad/s, and is trimmed with very little collective or lateral cyclic pitch. The differential ailerons are set to $-1°$, which allows the main rotor to trim with a roll moment, allowing slightly increased lift generation on the advancing side where it is efficient to do so. The main rotor therefore has a power requirement of only 145 hp, and the majority of the vehicle's 2,822 hp total power requirement is used by the collective propellers to overcome rotor and fuselage drag with 3,750 lbs of collective thrust.

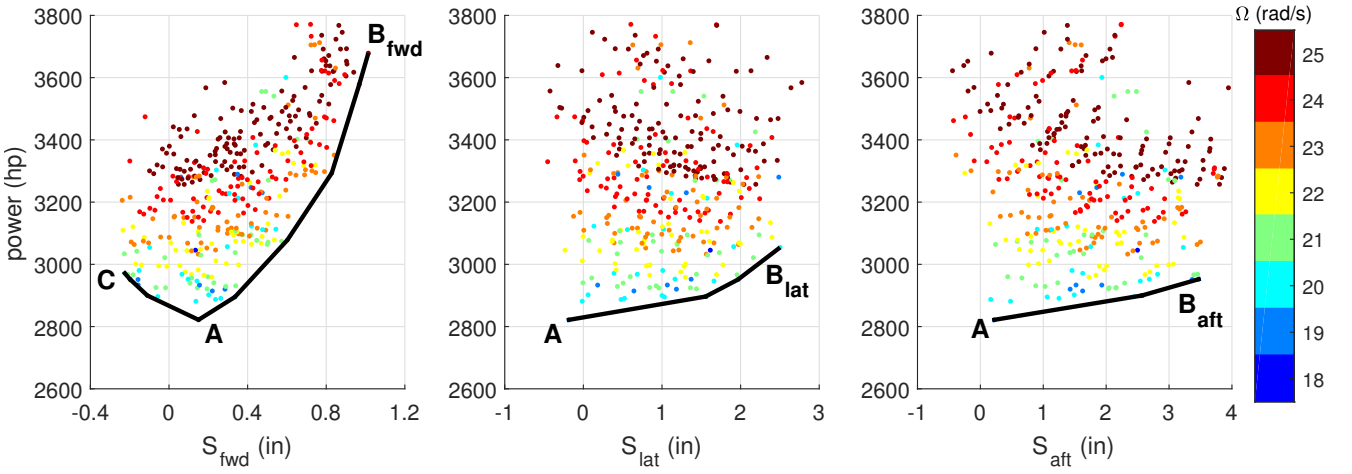

Fig. 14. Variation of trim state power (hp) due to servo position, and colored by rotor speed (rad/s) at 200 kts

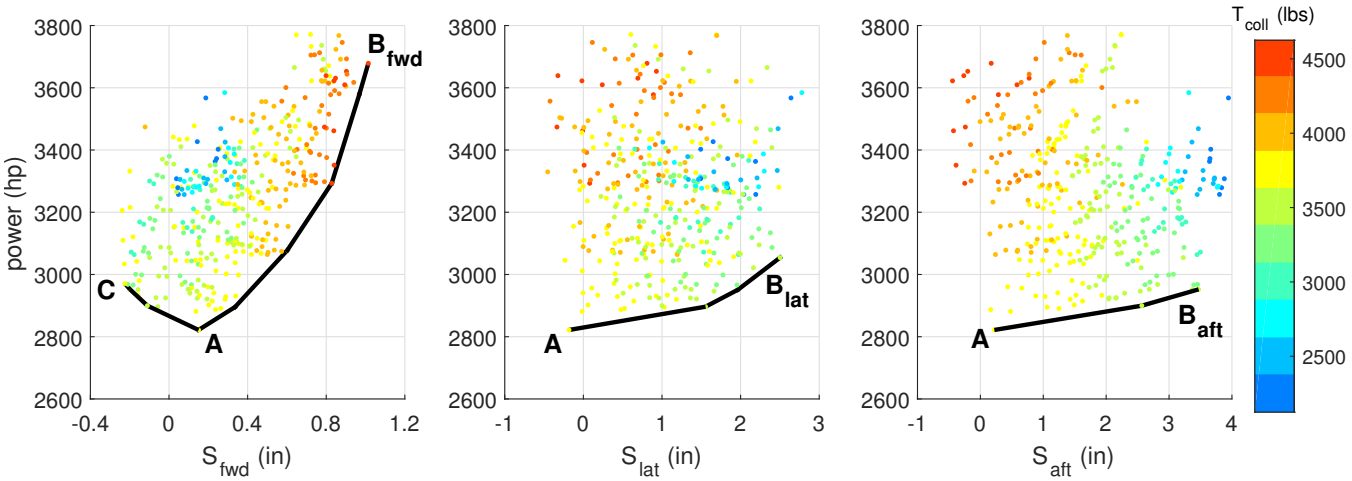

Fig. 15. Variation of trim state power (hp) due to servo position, and colored by collective auxiliary thrust (lbs) at 200 kts

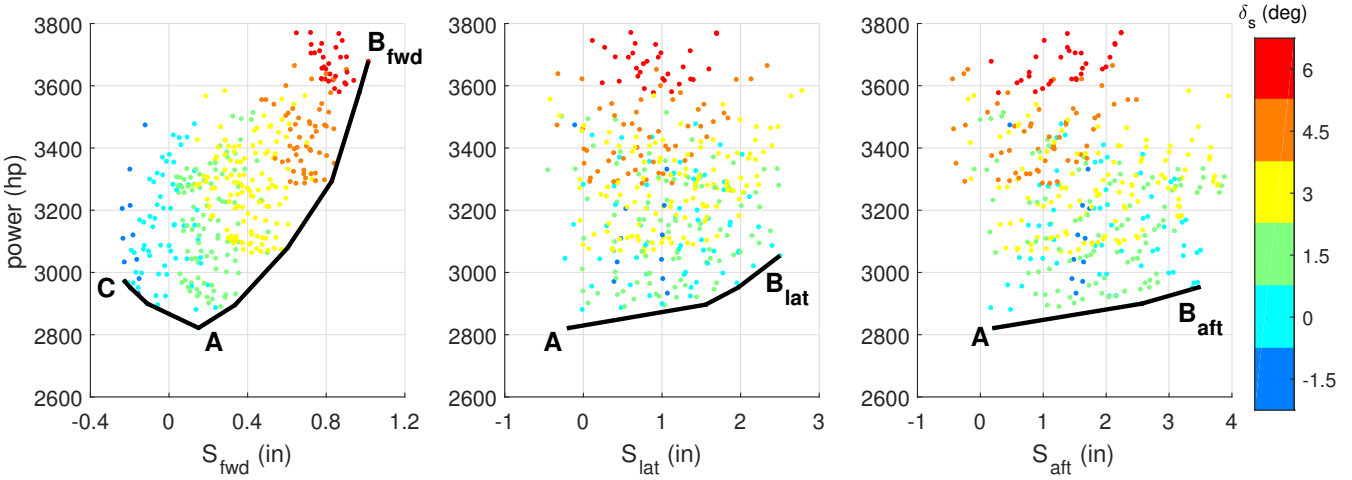

Fig. 16. Variation of trim state power (hp) due to servo position, and colored by stabilator pitch (°) at 200 kts

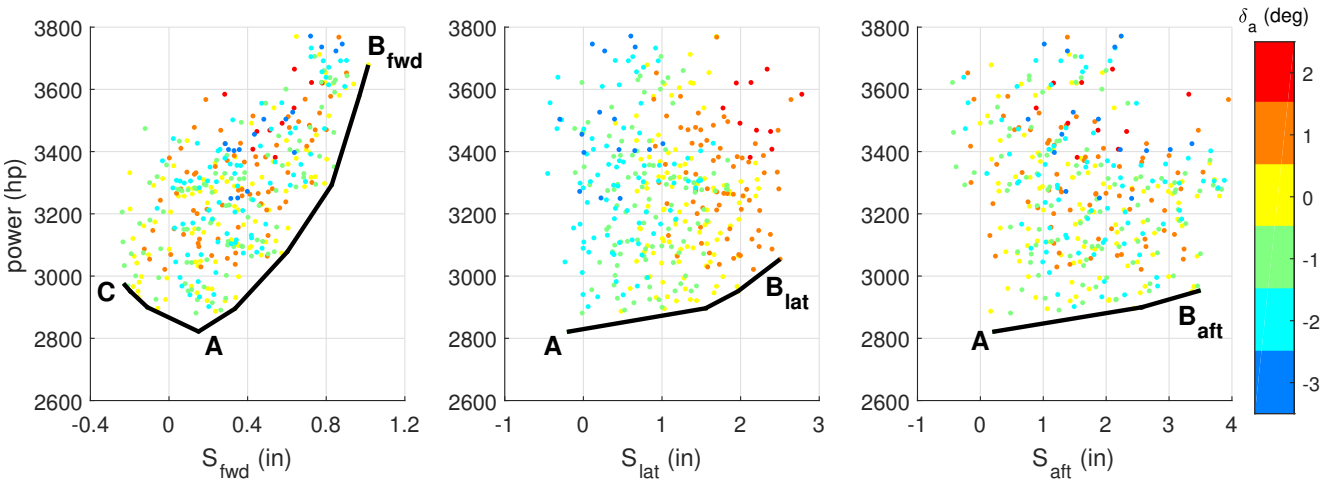

Fig. 17. Variation of trim state power (hp) due to servo position, and colored by differential aileron (°) at 200 kts

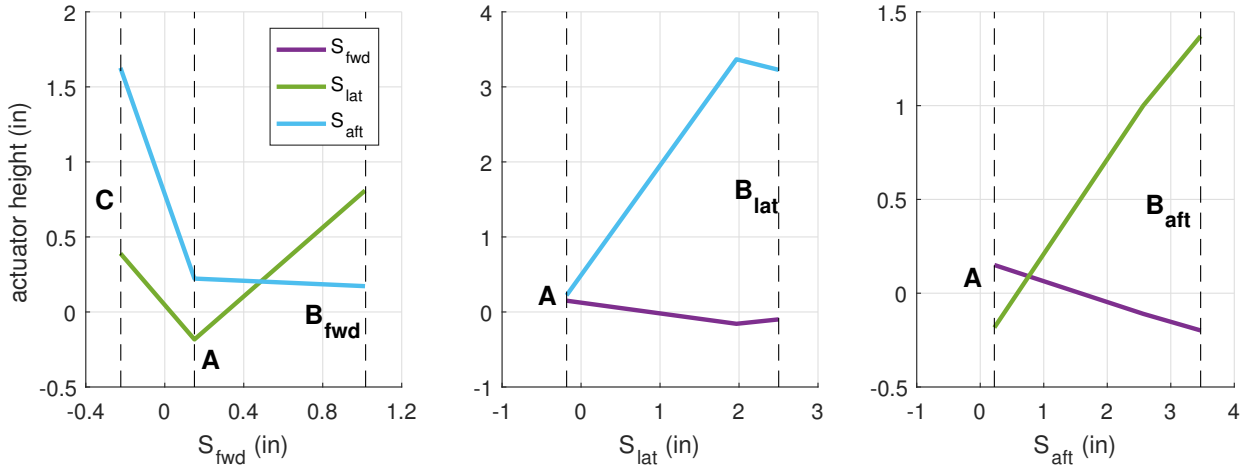

Fig. 18. Variation of remaining servos along the Pareto front of minimum power for a fixed servo at 200 kts

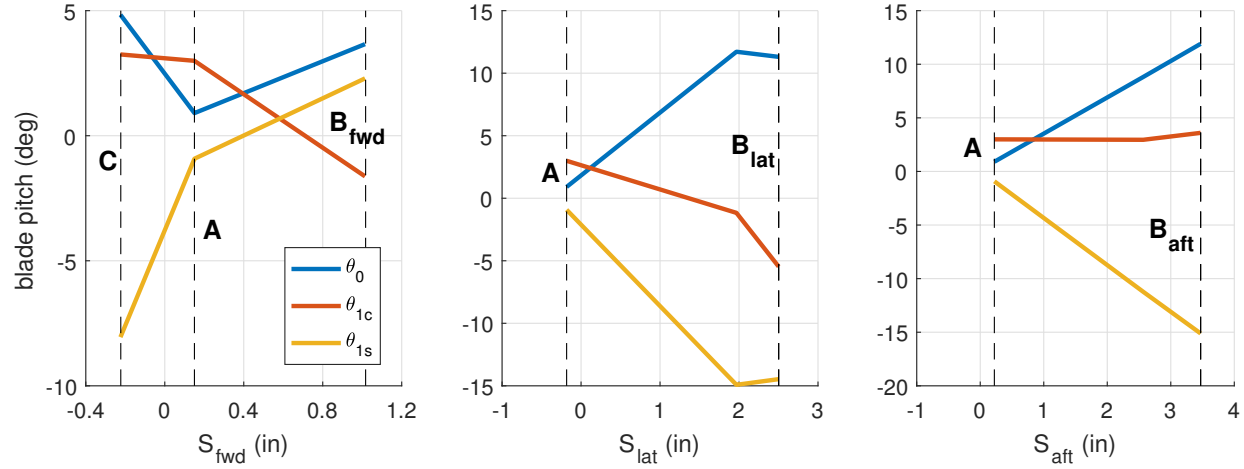

Fig. 19. Resultant blade pitches along the Pareto front of minimum power for a fixed servo at 200 kts

Table 6. Trimmed Pareto front limits at 200 kts

	A	B_{fwd}	B_{lat}	B_{aft}	C
S_{fwd}	0.15"	**1.01"**	−0.10"	−0.20"	**−0.22"**
S_{lat}	**−0.18"**	0.81"	**2.50"**	1.37"	0.39"
S_{aft}	**0.22"**	0.17"	3.23"	**3.47"**	1.63"
θ_0	0.9°	3.7°	11.3°	11.9°	4.8°
θ_{1c}	3.0°	−1.6°	−5.5°	3.6°	3.2°
θ_{1s}	−0.9°	2.3°	−14.5°	−15.1°	−8.1°
Ω	19 rad/s	25 rad/s	20 rad/s	19 rad/s	20 rad/s
T_{coll}	3,750 lbs	4,500 lbs	3,500 lbs	3,500 lbs	3,750 lbs
δ_s	0°	6°	0°	0°	−1.5°
δ_a	−1°	0°	1°	−1°	−1°
ϕ	−1.0°	0.3°	1.5°	−1.3°	−0.7°
α	1.7°	−2.3°	1.2°	1.2°	2.5°
β_0	0.5°	1.8°	1.4°	1.5°	0.2°
β_{1c}	−0.4°	−6.2°	4.2°	4.8°	4.8°
β_{1s}	3.4°	−1.7°	−5.4°	3.5°	3.7°
β_{min}	−2.9°	−4.6°	−5.5°	−4.4°	−5.9°
P_{rotor}	145 hp	391 hp	575 hp	473 hp	294 hp
P_{total}	2,822 hp	3,679 hp	3,054 hp	2,952 hp	2,971 hp
Main Rotor Forces and Moments (lbs) or (lbs-ft)					
Lift	4,088	11,774	5,614	5,607	2,689
Drag	420	1,511	237	238	306
Pitch Mom.	7,182	47,034	−24	−703	−5,803
Roll Mom.	10,662	330	−11,098	10,497	−10,452
Wing Forces and Moments (lbs) or (lbs-ft)					
Lift	14,719	7,077	13,657	13,663	16,304
Roll Mom.	−10,826	−1	10,815	−10,814	10,843
Stabilator Moments (lbs-ft)					
Pitch Mom.	−27,922	−60,632	−19,302	−19,339	−16,290

Forward Actuator

As the forward actuator (S_{fwd}) increases along the Pareto front from A to B_{fwd} in Figures 18 and 19, similar trends to those in Figures 11 and 12 are observed. Longitudinal cyclic pitch increases from −0.9° to 2.3°, collective pitch increases from 0.9° to 3.7°. At 100 kts, the majority of the S_{fwd} range came from longitudinal cyclic pitch with collective pitch actually reducing, while at 200 kts, both controls contribute similarly. With the longitudinal cyclic pitch increased, the main rotor flaps back −6.2°, which would be more extreme if not for the 6 rad/s increase in rotor speed. Since the baseline trim state at 200 kts offloaded the rotor to a 20% lift share, an increase in collective pitch can be tolerated to shift lift to the rotor. In total, the rotor drag increases to 1,511 lbs, and rotor lift nearly triples to 11,774 lbs as the rotor lift share is increased to 59%. As with 100 kts, stabilator pitch and vehicle pitch attitude are the key controls used to maximize S_{fwd} at 200 kts, as seen in Figure 20. Attempts to increase either longitudinal pitch beyond B_{fwd} would likely produce a violation of the constraint from Table 2. Increases to rotor speed also cannot be tolerated, as at 200 kts, the advancing blade tip Mach number would exceed 0.89.

At 100 kts, longitudinal cyclic was able to be set to −14.7° without violated flapping constraints. Trim state C at 200 kts not only has twice the free-stream velocity, but a 2 rad/s rotor speed reduction, and thus can only reduce longitudinal cyclic pitch to −8.1° before the minimum flap angle is −5.9°. Attempts to reduce either collective or longitudinal pitch further than C would produce a violation of the constraint from Table 2. As with 100 kts, the collective pitch increases greatly from trim state A to B_{fwd} as the vehicle pitch and rotor flapping tilt nose-down, such that a component of the free-stream velocity is added to the inflow of the rotor.

From the lowest value of S_{fwd} at trim state C to the upper limit at B_{fwd}, the actuator height varies by 1.23", from −0.22" to 1.01". At 100 kts, the total variation was 1.73", and was accomplished solely through increase in longitudinal cyclic pitch, and trimmed over an 8.5° increase in vehicle pitch attitude, and 24° increase in stabilator pitch. At 200 kts, longitudinal pitch is still the dominant contributor to S_{fwd} variation at the lower end of the Pareto front relative to trim state A. With a much higher range of lift capable of being shifted between the rotor and wing at high speeds, the collective pitch is also used to increase S_{fwd} relative to the low power trim state. Relative to 100 kts, the total S_{fwd} range is smaller due to the imposition of advancing blade tip Mach number constraints on the upper limit, and by a greater propensity for excessive

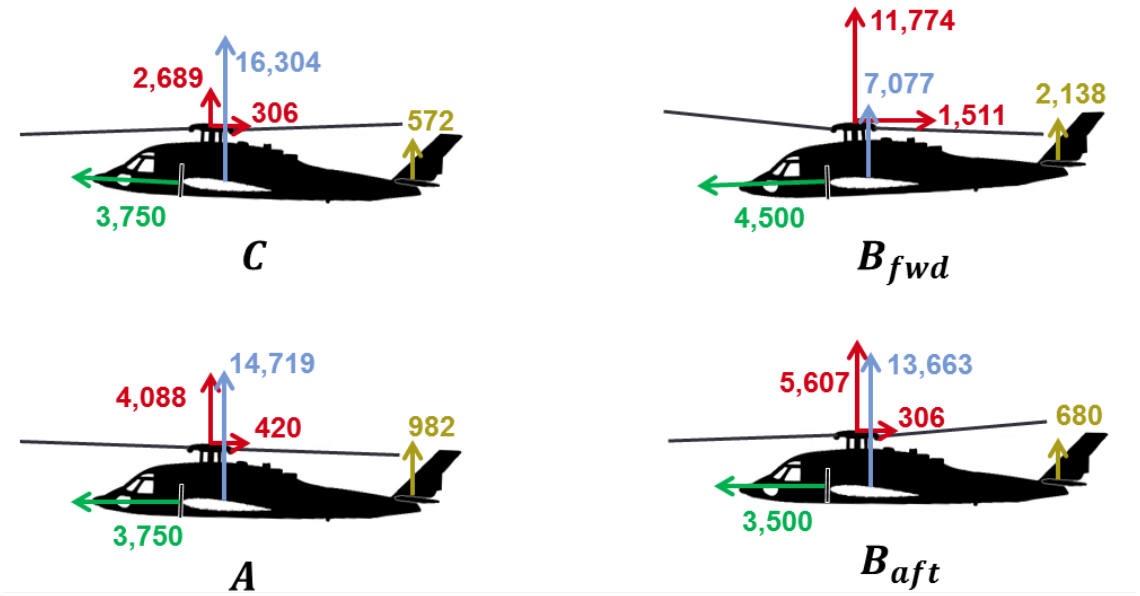

Fig. 20. Free body diagrams comparing major subsystem forces (lbs) at 200 kts (vehicle pitch attitude and blade flapping angles to scale)

flapping for all trim states with lower rotor speed.

Aft Actuator

For S_{aft} variation in Figures 14 – 17, trim state A is coincidental with the minimum height of the Pareto front, and the maximum is labeled B_{aft}. From Table 6 and Figures 18 and 19, moving from trim state A to B_{aft} increases S_{aft} by 3.25" as longitudinal cyclic pitch decreases from $-0.9°$ to $-15.1°$ and collective pitch increases from 0.9° to 11.9°. The vehicle pitch attitude of trim states A and B_{aft} only differ by 0.5°, compared to the 4.8° of difference along the S_{fwd} Pareto front. This shows agreement with the 100 kts conclusions, which had the greatest correlation between S_{aft} and collective propeller thrust, and between S_{fwd}, vehicle pitch attitude, and stabilator pitch. At 200 kts the only variation in redundant controls between trim state A and B_{aft} at either limit of the S_{aft} Pareto front is a 250 lbs reduction in collective propeller thrust.

Further implementation of collective propeller thrust to increase S_{aft} range would produce violation of minimum cyclic pitch beyond trim state A and of minimum longitudinal cyclic pitch beyond trim state B_{aft}. While B_{fwd} was able to reduce longitudinal cyclic relative to A, the reduced vehicle pitch attitude resulted in a higher collective pitch, and a slightly higher S_{aft} of 0.17", ultimately counteracting the benefits of the reduced longitudinal cyclic.

Lateral Actuator

For S_{lat} variation in Figures 14 – 17, trim state A is coincidental with the minimum height of the Pareto front. In Eqn. 2, the S_{lat} height is related to the blade pitch as proportional to the difference of collective pitch and lateral cyclic pitch. Therefore, minimization of S_{lat} is achieved through minimization of collective pitch, and maximization of lateral flapping. At trim state A, the lateral cyclic pitch is 3.0° to generate 3.4° of lateral flapping. The lateral flapping of the rotor positions a component of the rotor thrust laterally to produce a $10,662$ lbs-ft roll moment, which acts upward on the advancing side. Increased lift on the advancing side where there is high dynamic pressure is beneficial for power, which is why trim state A uses $-1°$ of differential ailerons. In terms of S_{lat}, the high wing lift-share and rotor roll moment that permits lift generation on the advancing side of the aircraft contribute to a low collective pitch. Through these mechanisms, trim state A is both the power optimal trim state, and the minimum S_{lat} trim state of -0.18".

As shown in Figure 17, there is a correlation between increase in differential aileron deflection and increase in S_{lat}. This can be verified by comparing trim state B_{lat} against A, from Table 6. B_{lat} trims with a substantial increase in S_{lat} of 2.68" relative to trim state A, which manifests as a large increase in collective pitch and a reduction in lateral cyclic pitch (Eqn. 2). The lateral cyclic pitch is reduced from 3.0° to $-5.5°$ to switch the direction of lateral blade flapping, from 3.4° to $-5.4°$. The most significant change to the rotor force and moment production is to the roll moment, which switches sign entirely from $10,662$ to $-11,098$ lbs-ft, and is compensated by the ailerons. The collective pitch increase from 0.9° to 11.3° produces little added forces or moments due to the increased rotor inflow with forward flapping.

TOTAL RECONFIGURABLE FAILURE RANGES

Using the main rotor pitch control limits in Table 2 and the relationships between pitch control and servo heights given by Eqns. 1 – 3, the corresponding maximum and minimum servo limits can be determined. S_{fwd} can range from -1.87" to 4.29", S_{lat} can range from -0.86" to 3.55, and S_{aft} can range from -2.07" to 4.46". In addition to these limits, Figure 21 also shows the limits of trimmed flight attainable using the reconfiguration strategies outlined in prior sections. The percentage of the total limits that can be successfully reconfigured for trim are given in Table 7

Table 7. Percent of total servo range that can be compensated for using redundant controls

	Hover	100 kts	200 kts
S_{fwd}	6%	28%	20%
S_{lat}	10%	63%	61%
S_{aft}	12%	56%	50%

With rotor speed as the only viable option for reconfiguration in hover, the hover trim states can only tolerate a narrow range of locked actuator failures, between 6% and 12% of the total range. Increasing the sensitivity of the ailerons and stabilator at 100 kts increases the range reconfigurable failures to between 28% and 63% of the limits. At 200 kts, the reduced rotor speeds and increased sensitivity of rotor flapping to main rotor pitch imposes tighter constraints from blade flapping, and thus the range of tolerable failures reduces slightly to 20% to 50%.

As longitudinal pitch becomes more negative and flaps forward, less excess forces and moments are produced by also increasing the collective pitch as the free-stream velocity adds to inflow. Because it is proportional to the difference of collective and longitudinal cyclic pitch, the aft servo covers a larger range of tolerable failures than the forward servo. The forward servo, is minimized by decreasing both collective and longitudinal pitches, which produces greater excess of blade flapping and rotor forces and moments which are more difficult to compensate for with redundant controls. The limits on lateral pitch and flapping are tighter than on longitudinal flapping, so the maximum travel in Figure 21 is the smallest, and the percentages of reconfigurable states in Table 7 are the largest.

CONCLUSIONS

Control of a helicopter's main rotor is typically accomplished through use of three hydraulic actuators that act on the non-rotating swashplate and position it to achieve any combination of collective and cyclic blade pitch. Failure of one of these servos can happen through loss of hydraulic pressure or by impingement of the piston within the hydraulic cylinder. On a conventional helicopter, this is avoided by including a redundant hydraulic system for each actuator assembly, as the lack of redundant effectors could cause catastrophic failure. For a compound helicopter, a range of failed servo states (by piston impingement) are examined at hover, 100 kts, and 200 kts, to show the extent to which the compound effectors are capable of reconfiguration after failure.

After the loss of control of any of the three main rotor actuators, the main rotor blade pitch is no longer fully controllable. Instead a subset of the blade pitches are available to the pilot subject to the position of the locked actuator, and control of the remaining two actuators produces a coupled effect across collective, lateral and longitudinal pitches. In hover, the compound helicopter is capable of trimming a locked actuator with little change to the state of the vehicle, by replacing control of the locked servo with control of rotor speed. Relative to the maximum travel of the actuators, between 6 – 12% of the range can be successfully reconfigured.

At forward flight speeds, each of the three actuators produces a different result on the trimmed aircraft due to the non-axisymmetry of the rotor. The sensitivity of the wing and horizontal stabilator at forward flight speeds is greatly increased, and the range of feasibly trimmed fixed actuator positions triples compared to hover.

For the forward actuator, which acted at $\psi = 90°$, a 20 – 28% range of locked positions are accommodated by allowing the main rotor to produce a net longitudinal cyclic pitch and blade flapping angle, which produces excess forces and moments trimmed primarily by the stabilator, the vehicle pitch attitude (for wing lift), and to a lesser extent the collective propeller thrust.

For the aft actuator, which acted at $\psi = 270°$, an even larger 50 – 56% range of locked failures are accommodated by allowing the main rotor to produce net collective pitch and longitudinal cyclic pitch, which produces forces and moments that are trimmed primarily by the collective propeller thrust, and to a lesser extent the stabilator pitch.

The lateral actuator acts at $\psi = 180°$, and is most directly trimmed by allowing lateral cyclic pitch and flapping, and countering the net roll moment with an opposing one by the differential ailerons in trim. Further benefits can also be attained by allowing collective pitch variation, bringing the tolerable range of reconfiguration to 61 – 63% of the maximum servo limits.

Author contact: Jean-Paul Reddinger, reddij2@rpi.edu; Farhan Gandhi, fgandhi@rpi.edu

REFERENCES

[1]Eslinger, R. A., and Chandler, P. R.., "Self-Repairing Flight Control System Program Overview," Proceedings of the IEEE 1988 National Aerospace and Electronics Conference, Vol. 2, May 23–27, 1988, pp. 504–511.
doi: 10.1109/NAECON.1988.195055

[2]Stewart, J. F., and Shuck, T. L.., "Flight-Testing of the Self-Repairing Flight Control System Using the F-15 Highly Integrated Digital Electronic Control Flight Research Facility,"

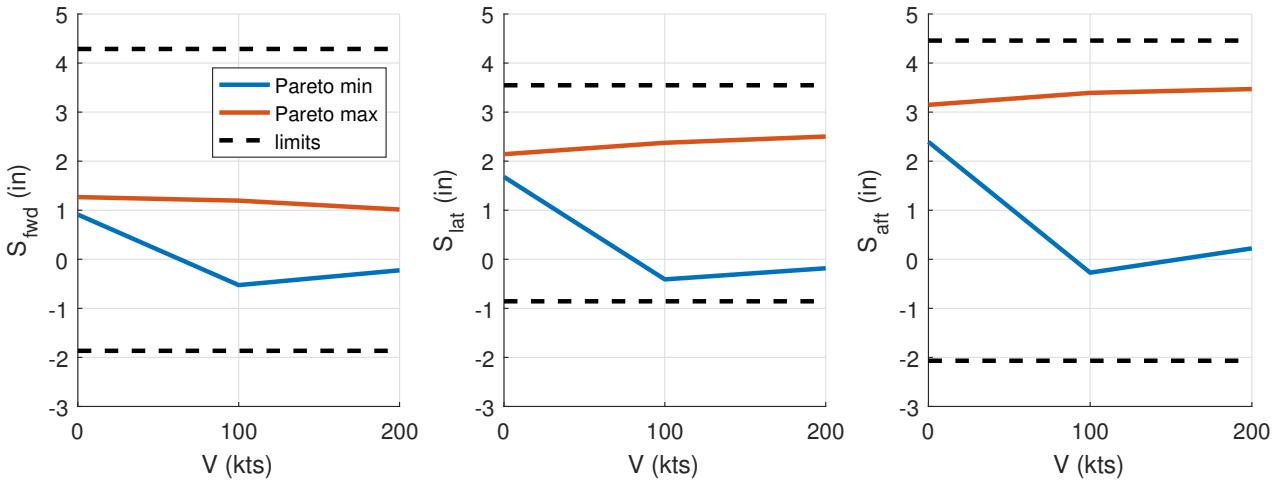

Fig. 21. Comparison of trimmable servo failures over the Pareto fronts at each flight speed

NASA TM-101725, NASA Ames Research Center, Edwards, CA, Aug., 1990.

[3]Bodson, M., and Groszkiewicz, J. E., "Multivariable Adaptive Algorithms for Reconfigurable Flight Control," *IEEE Transactions on Control Systems Technology,* Vol. 5, (2), March 1997.
doi: 10.1109/87.556026

[4]Brinker, J. S., and Wise, K. A., "Flight Testing of Reconfigurable Control Law on the X-36 Tailless Aircraft," *Journal of Guidance, Control, and Dynamics,* Vol. 24, (5), 2001, pp. 903–909.
doi: 10.2514/2.4826

[5]Heiges, M. W., "Reconfigurable Controls for Rotorcraft–A Feasibility Study," *Journal of the American Helicopter Society,* Vol. 42, (3), 1997, pp. 254–263.
doi: 10.4050/JAHS.42.254

[6]Enns, R., and Si, J., "Helicopter Flight-Control Reconfiguration for Main Rotor Actuator Failures," *Journal of Guidance, Control, and Dynamics,* Vol. 26, (4), 2003, pp. 572–584.
doi: 10.2514/2.5107

[7]Hess, R. A., "A Framework for Robust Rotorcraft Flight Control Design," *Journal of the American Helicopter Society,* Vol. 56, (2), 2011.
doi: 10.4050/JAHS.56.022004

[8]Sekula, M. K., and Gandhi, F., "Effects of Auxiliary Lift and Propulsion on Helicopter Vibration Reduction and Trim," *Journal of Aircraft,* Vol. 41, (3), May–Jun. 2004, pp. 645–656.
doi: 10.2514/1.496

[9]Gandhi, F., and Sekula, M. K., "Helicopter Vibration Reduction using Fixed-System Auxiliary Moments," *AIAA Journal,* Vol. 42, (3), Mar. 2004, pp. 501–512.
doi: 10.2514/1.575

[10]Sekula, M. K., and Gandhi, F., "Helicopter Vibration and Rotor Power Reduction through Horizontal Tail Incidence Angle Control," American Helicopter Society 60^{th} Annual Forum, Baltimore, MD, Jun. 7–10, 2004.

[11]Gandhi, F., and Sekula, M. K., "Helicopter Horizontal Tail Incidence Control to Reduce Rotor Cyclic Pitch and Blade Flapping," American Helicopter Society 60^{th} Annual Forum, Baltimore, MD, Jun. 7–10, 2004.

[12]Reddinger, J. P., and Gandhi, F., "Performance and Hub Vibrations of an Articulated Slowed-Rotor Compound Helicopter at High Speeds," American Helicopter Society 71^{st} Annual Forum, Virginia Beach, VA, May 5–7, 2015.

[13]Reddinger, J. P., and Gandhi, F., "Physics-Based Trim Optimization of an Articulated Slowed-Rotor Compound Helicopter in High-Speed Flight," *Journal of Aircraft,* Vol. 52, No. 6 (2015), pp. 1756–1766.
doi: 10.2514/1.C032939

[14]Barron, H. M., Brentner, K, Horn, J. F., Ozdemir, G. T., and Thorsen, A. T., "Acoustic Analysis of Compound Helicopters with Trim Variations," American Helicopter Society 69^{th} Annual Forum, Phoenix, AZ, May 21–23, 2013.

[15]Ozdemir, G. T., Horn, J. F., and Thorsen, A., "In-Flight Multi-Variable Optimization of Redundant Controls on a Compound Rotorcraft," AIAA Guidance, Navigation, and Control Conference, Boston, MA, August 19–22, 2013.

[16]Ozdemir, G. T., and Horn, J. F., "Simulation Analysis of a Flight Control Law with In-Flight Performance Optimization," American Helicopter Society 68^{th} Annual Forum, Fort Worth, TX, May 1–3, 2012.

[17]Thorsen, A., Horn, J. F., and Ozdemir, G. T., "Use of Redundant Controls to Enhance Transient Response and Handling Qualities of a Compound Rotorcraft," American Helicopter Society 70^{th} Annual Forum, Montréal, QC, Canada, May 21–23, 2014.

[18]Yeo, H., Bousman, W. G., and Johnson, W., "Performance Analysis of a Utility Helicopter with Standard and Advanced Rotors," *Journal of the American Helicopter Society,* Vol. 49, (3), Jul. 2004, pp. 250–270.
doi: 10.4050/JAHS.49.250

[19]Ormiston, R. A., "Low-Disk Loading Compound Rotorcraft for High Speed and Aerodynamic Efficiency," AHS, AIAA, SAE, RAeS International Powered Lift Conference Proceedings, Philadelphia, PA, Oct. 5–7, 2010.

[20]Moodie, A. M., and Yeo, H., "Design of a Cruise-Efficient Compound Helicopter," *Journal of the American Helicopter Society,* Vol. 57, (3), Jul. 2012, pp. 1–11.
doi: 10.4050/JAHS.57.032004

[21]Peters, D. A., and He, C. J., "Correlation of Measured Induced Velocities with a Finite-State Wake Model," *Journal of the American Helicopter Society,* Vol. 36, (3), Jul. 1991, pp. 59–70.
doi: 10.4050/JAHS.36.59

[22]Saberai, H., Khoshlahjeh, M., Ormiston, R., and Rutkowski, M. "Overview of RCAS and Application to Advanced Rotorcraft Problems," AHS 4^{th} Decennial Specialists' Conference on Aeromechanics, San Francisco, CA, Jan. 21–23, 2004.

[23]Silbaugh, B., Kang, H., Floros, M., and Singh, R. "Investigation of RCAS–CAMRAD II UH60 Structural Dynamics Model Correlation," American Helicopter Society 70^{th} Annual Forum, Montréal, QC, Canada, May 21–23, 2014.

[24]Jain, R., Yeo, H., Ho, J. C., and Bhagwat, M. "An Assessment of RCAS Performance Prediction for Conventional and Advanced Rotor Configurations," American Helicopter Society 70^{th} Annual Forum, Montréal, QC, Canada, May 21–23, 2014.

[25]United States Army Aviation Warfighting Center. *UH-60 Flight Control and Hydraulic Systems,* 4745-3, Fort Rucker, AL, Feb. 2008.

[26]United States Army Aviation Warfighting Center. *UH-60 Flight Control and Hydraulic Systems,* 4747-9, Fort Rucker, AL, Jul. 2002.